THE JOURNAL OF PHYSICAL CHEMISTRY C
A JOURNAL OF THE AMERICAN CHEMICAL SOCIETY

pubs.acs.org/JPCC

Article

Dehydrofluorination as a Residue-Free Selective Route to C−C Bond Formation at Metal Surfaces

Jonathan Viereck, Yang Zhang, Elena Galoppini, Robert A. Bartynski, and Sylvie Rangan*

Cite This: J. Phys. Chem. C 2022, 126, 6249−6257

Read Online

ACCESS | Metrics & More | Article Recommendations | Supporting Information

ABSTRACT: Directing covalent on-surface polymerization of molecular precursors through rational synthetic design has been impaired by the lack of control over reaction sites and by limited chemical routes to covalent bond formation between precursors, resulting in limited control of the outcomes and parasitic surface reaction byproducts. Here we investigate the mechanism of a recently reported chemical route to C−C bond formation: dehydrofluorination on metal surfaces. We demonstrate that this chemical route, involving specifically C−H/F−C pairs, favors the elimination of HF in the gas phase as a single step, therefore eliminating reaction byproducts at the surface of metals. Unlike dehalogenation, we find that the remarkable selectivity of the dehydrofluorination reaction renders this C−C bond formation strategy chemoselective as well as potentially regioselective, if employed with a properly designed molecular precursor. Additionally, we demonstrate that the catalytic role of the metal substrate can be used to steer reaction pathways and select between dehydrofluorination and dehydrogenation reaction. For these reasons, the dehydrofluorination reaction, largely unexplored on metal surfaces, could become a valuable tool for on-surface synthesis.

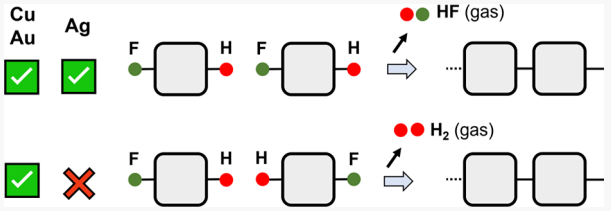

INTRODUCTION

On-surface synthesis, involving directing covalent C−C bond formation for controlled on-surface polymerization, through rational design of organic molecular precursors has become a major synthetic strategy in organic electronics and in the search for emergent topological materials.[1,2] Such an approach starts with the deposition of an organic molecular precursor on a surface, typically a single crystal metal, followed by a multistep process involving sequential intra- and intermolecular C−C bond formation reactions among molecular precursors. However, such processes exhibit limited chemo- and regioselectivities over the reaction sites and chemical routes to covalent bond formation, resulting in a wide variety of products linked in disordered arrays. Therefore, there is the need to develop an "on-surface chemical toolbox" that can be used to steer self-assembly and intra- and intermolecular covalent bond formation toward a desired highly ordered 2D organic material.

Several approaches to directing surface 2D polymerization have been explored with varying degrees of success. Copper-catalyzed aryl−aryl coupling, i.e., the Ullmann reaction,[3] has been adapted to various single crystal metal surfaces with a variety of aromatic hydrocarbons (benzene derivatives, polyacenes, fluorenes, or porphyrins) substituted with either chlorine, bromine, or iodine.[1,2,4−7] Homolytic cleavage of the carbon−halogen bond is activated either thermally or electronically, resulting in radical species which may recombine forming new C−C bonds. Moreover, because of the halogen-dependent dissociation temperature of the carbon−halide bond on metal surfaces (typically $T_I < T_{Br} < T_{Cl}$), some degree of selectivity can be achieved with "programmed" dehalogenation reactions resulting in sequential Ullmann coupling steps.[8,9] However, cleavage of the carbon−halogen bond does not immediately lead to desorption of the halogen atoms from the surface: there is typically a temperature window where the radicals and adsorbed halogens coexist on the surface. While the halogen desorption temperature can be relatively low, the fact remains that while covalent coupling between radicals takes place the adsorbed halogens may get in the way during the radical diffusion step or the growth of a polymer island.[10−12]

Another common route for C−C bond formation is the dehydrogenation reaction on a metal surface, involving the thermally activated cleavage of two adjacent C−H bonds.[13−16] An attractive feature of this approach is that it produces H_2 gas, which does not remain on the surface. A combination of both Ullmann coupling and dehydrogenation reactions has found important use for the on-surface molecular assembly and subsequent ring closure required for the on-surface synthesis of polycyclic aromatic compounds such as graphene nanoribbons (GNRs).[16,17]

Received: January 28, 2022
Revised: March 15, 2022
Published: March 31, 2022

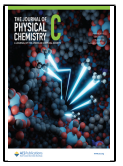

https://doi.org/10.1021/acs.jpcc.2c00712
J. Phys. Chem. C 2022, 126, 6249−6257

Recently, following the observation that thermal activation of C−H and F−C bonds in close proximity on an Al_2O_3 substrate catalyst leads to intramolecular C−C bond formation,[18,19] dehydrofluorination has been utilized for nanostructure growth on a TiO_2(011) surface.[20,21] It is proposed that the metal centers of this oxide surface polarize the C−F bonds and act as a catalyst for F abstraction, ultimately leading to dehydrofluorination and C−C bond formation.[22] H and F byproducts of the HF elimination process remain adsorbed on the surface and recombine with surface atoms leading to either surface-adsorbed H_2O or gas phase $TiOF_2$, the latter of which erodes the surface.[20] Attempts to thermally induce dehydrofluorination reactions on a metal surface, Au(111), have led to a variety of reports indicating either the absence of a catalytic effect resulting in no C−C bond formation,[20,23] C−C bond formation with no apparent chemoselectivity between initial molecular bond pairs C−H/C−H, C−H/C−F, or C−F/C−F,[24] or most recently a very efficient and selective intermolecular C−C bond formation.[25] In addition, some evidence of regioselective C−C bond formation via dehydrofluorination has been reported for a fluorinated corrole derivative on Ag(111).[26] Independent of C−C bond formation, the stability of the C−F bond on metal surfaces has been studied in the course of making edge-fluorinated GNRs on Au(111).[27−29] In these studies, it is proposed that F can be replaced by an H migrating from a neighboring molecular site that just underwent a classical dehydrogenation reaction upon C−C bond formation.

Here, we are seeking insights into the fundamental aspects of the dehydrofluorination reaction on metal surfaces using a custom-made fluorinated zinc tetraphenylporphyrin (ZnTPP) precursor, ZnTPP-m-oF8, shown in Figure 1: in this molecule,

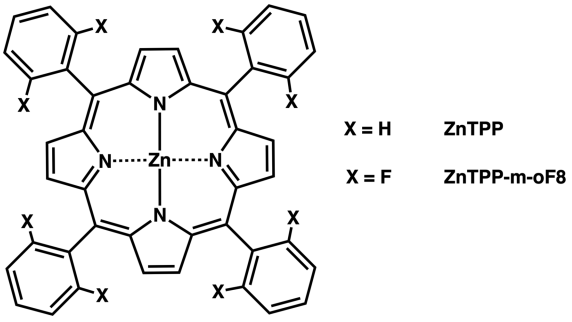

Figure 1. Molecular structures of ZnTPP-o-mF8 and ZnTPP.

fluorine substituents are placed at the two ortho positions of each meso-phenyl ring. In this work, molecular precursors are adsorbed onto single crystal metal surfaces at various coverages and subsequently annealed to trigger on-surface C−C bond formation. The chemical environment of the surface products is investigated by using X-ray photoelectron spectroscopy (XPS) aided by density functional theory (DFT) calculations, while their molecular structure and resulting connectivity are studied by using scanning tunneling microscopy (STM). Finally, the products eliminated in the gas phase upon C−C bond formation are monitored by using temperature-programmed desorption (TPD). Thus, a detailed picture of the chemical transformations upon annealing on the metal surface is obtained.

Dehydrofluorination reactions of ZnTPP-m-oF8 on two single crystal metal surfaces, Cu(100) and Ag(100), indicate that the mechanism at play here is qualitatively different from typical dehalogenation reactions. As the reaction involves preferentially C−H/F−C pairs, rather than C−H/H−C or C−F/F−C pairs, it appears more chemoselective than other homocoupling routes involving dehalogenation or dehydrogenation and leads to either intra- or intermolecular C−C bond formation with HF loss to the gas phase. The intermolecular reaction occurs about 100 °C higher in temperature than the facile intramolecular reaction, as the intermolecular reaction requires diffusion to bring reaction sites on two different molecules into close proximity. Significant H_2 elimination is measured only for annealing temperatures above those resulting in HF elimination. Moreover, a comparison of the catalytic role of three metal substrates, Cu(100), Ag(100), and Au(111), on the C−C bond formation, using as precursors the simple ZnTPP and its fluorinated derivative ZnTPP-m-oF8, indicates that metal substrates can be used to steer reaction pathways and select between dehydrofluorination and dehydrogenation reaction.

EXPERIMENTAL METHODS

Sample Preparation. The Au(111), Ag(100), and Cu(100) surfaces were prepared with several cycles of Ar^+ sputter and anneals above 400 °C. ZnTPP-m-oF8 and ZnTPP molecules were deposited at room temperature by using a Knudsen cell held at 230 and 280 °C, respectively, after thorough degassing. Details of the molecular synthesis for ZnTPP-m-oF8 have been reported in a separate work.[30]

Temperature-Programmed Desorption Spectroscopy. Temperature-programmed desorption (TPD) measurements were performed in a UHV chamber with a base pressure better than 2×10^{-10} Torr equipped with sputtering, annealing, and molecular deposition sources for surface preparation. Molecular coverage was determined in XPS using a nonmonochromated source with a 1486.7 eV photon energy and a cylindrical mirror electron analyzer, with an overall energy resolution of 1 eV. We performed TPD with an annealing rate of 2 °C/s, using an SRS 200 RGA equipped with a Feulner cup, at a sample surface−cup aperture distance of ∼1 mm.

Electron Spectroscopies. Photoemission measurements were performed in an ESCALAB 250Xi equipped with a preparation chamber with a pressure better than 5×10^{-10} Torr allowing in situ deposition and annealing. Temperatures are measured with a thermocouple placed directly on the surface of the crystal. Core levels are measured with a 1486.7 eV photon energy with an energy resolution of 0.6 eV, while the valence band is measured with a 40.8 eV photon energy and the work function with a 21.2 eV photon energy, both with an energy resolution better than 0.1 eV. Inverse photoemission measurements were performed in a custom-made grating spectrometer with an incident 20.3 eV monochromatic electron source, resulting in an overall resolution of 0.6 eV of the conduction band spectra.

Electronic Structure. Electronic structure calculations were performed with the GAMESS(US) software package[31] by using Becke3−Lee−Yang−Par (B3LYP) three-parameter DFT theory.[32,33] Geometries of local minima on the potential energy surface were calculated with a 6-31G basis set.[34] The DOS spectra were obtained as a sum of the individual weighted electronic states convoluted with a Gaussian function of 0.7 eV full width at half-maximum (FWHM).

https://doi.org/10.1021/acs.jpcc.2c00712
J. Phys. Chem. C 2022, 126, 6249−6257

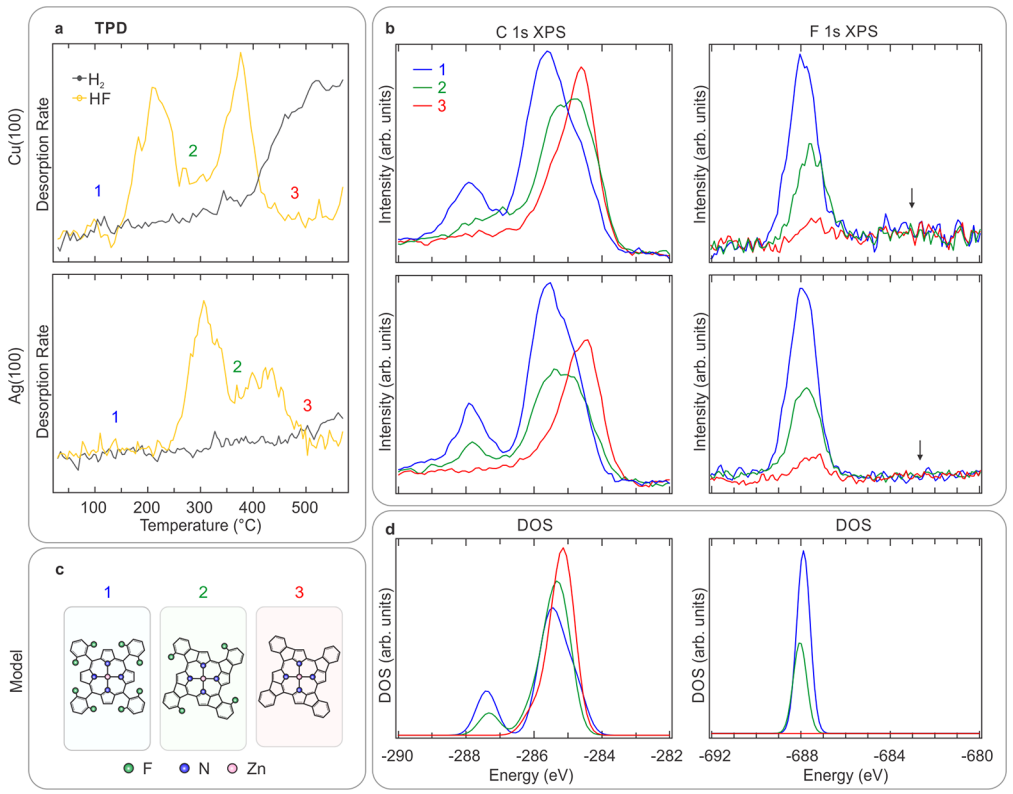

Figure 2. Reaction stages. Chemical transformations of molecular species and gas phase residual products upon annealing Cu(100) and Ag(100) single crystal surfaces, with initial coverages of a monolayer of ZnTPP-m-oF8. (a) TPD spectra indicate two HF elimination processes separated in temperature by ~100 °C, followed by H_2 loss only at higher temperatures. (b) C 1s and F 1s core levels measured before and after the HF loss indicate fluorine loss from the molecular adsorbate without metal fluoride formation at the surface. The typical metal fluoride region is indicated by arrows. Numbers 1, 2, and 3 indicate three reaction stages: before the first HF loss, before the second HF loss, and after the second HF loss, respectively. (c) Molecular models 1, 2, and 3, (see also the Supporting Information) corresponding to these reaction stages were chosen to calculate the C 1s and F 1s density of states spectra in (d), used for XPS C 1s and F 1s spectra analysis.

Scanning Tunneling Microscopy (STM). STM measurements were performed in an Omicron VT-SPM in constant current mode at room temperature under pressures better than 5×10^{-10} Torr. The chamber is equipped with sputtering, annealing, and in situ molecular deposition sources. Images were processed by using the WSxM software.[35] For the STM measurements, because of a combination of noise and drift during imaging, the uncertainties were conservatively estimated to be ±0.1 Å for heights, ±0.5 Å for lateral distances, and 3° for angles. Molecular coverage was also measured by XPS using a nonmonochromated source with a 1486.7 eV photon energy and a cylindrical mirror electron analyzer, with an overall energy resolution of 1 eV.

RESULTS AND DISCUSSION

Experimental Results. A self-assembled molecular monolayer of ZnTPP-m-oF8 was deposited on atomically clean and highly ordered Cu(100) and Ag(100) single crystal surfaces that were subsequently annealed at a rate of 2 °C/s while desorbing products were monitored by mass spectrometry, as shown in Figure 2a. Only two desorption products were found: HF and H_2. No significant desorption of F_2 was measured as shown in Figure S4. As indicated in Figure 2a, on both surfaces progressive annealing of a monolayer of ZnTPP-m-oF8 leads to two distinct HF desorption peaks which, as discussed below, are attributed to intra- and intermolecular HF elimination reactions. The TPD spectra suggest that the surface species can be characterized in three stages: (1) an as-deposited monolayer, (2) a layer measured after the first HF desorption peak, and (3) a layer measured after the second HF desorption peak. In addition, H_2 desorption was only observed for temperatures higher than 400 °C, i.e., above the temperature at which HF desorption is completed. Marked differences are observed on the two surfaces: (i) each of the desorption peaks occur typically at lower temperatures on Cu(100) than on Ag(100); (ii) although the integrated intensity of the intra- and intermolecular HF desorption peaks from a given surface are approximately equal, the peak widths are surface dependent; (iii) the peak temperature separation is smaller on Ag(100) than on Cu(100), leading to a temperature range where the two HF desorption peaks overlap. These differences provide important clues about the reaction mechanism.

XPS core level spectra were measured before and after sequential anneals of a ZnTPP-m-oF8 monolayer on Cu(100) and Ag(100) (all of which are shown in the Supporting Information). A subset of these core levels is presented in Figure 2b, corresponding to stages 1, 2, and 3 of the surface reactions, as indicated in the TPD spectra of Figure 2a. In Figure 2b, the C 1s and F 1s core levels, each normalized to either the Cu 2p or Ag 3d intensity to account for possible molecular desorption, are presented for each reaction stage. As a useful comparison, in Figure 2d the calculated density of states (DOS) for the C 1s and F 1s ground state core levels are presented for each of the model compounds shown in Figure 2c.

https://doi.org/10.1021/acs.jpcc.2c00712
J. Phys. Chem. C 2022, 126, 6249−6257

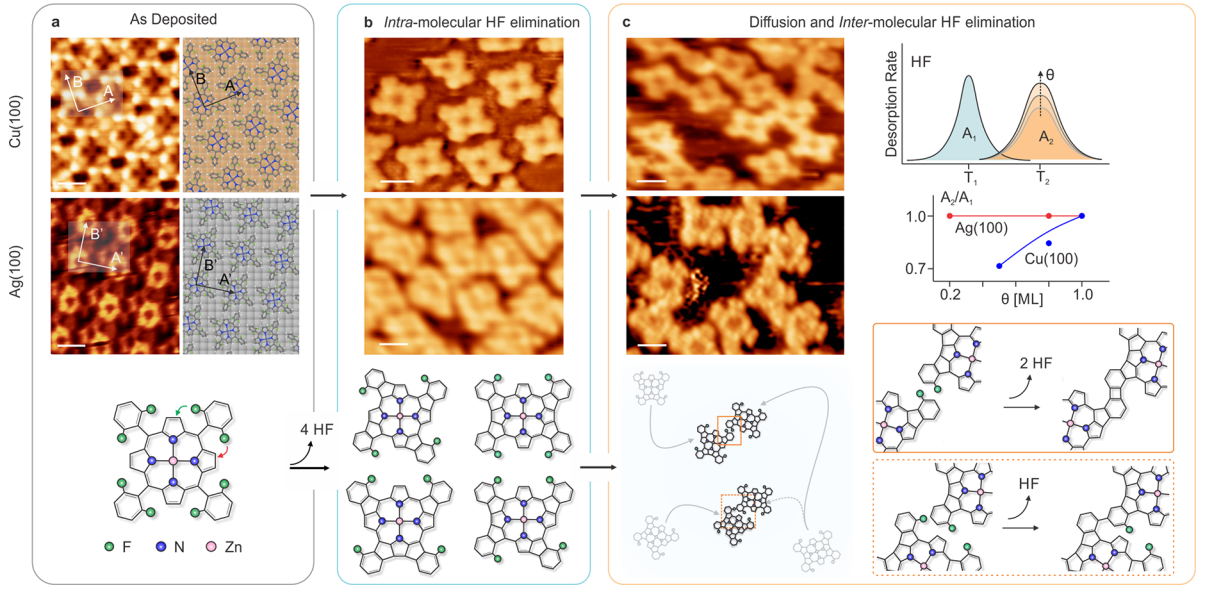

Figure 3. Proposed mechanism for dehydrofluorination on metal surfaces. (a) STM images indicate that as-deposited layers of ZnTPP-m-oF8 self-assemble intact on Cu(100) and Ag(100), in nearly square arrays favoring phenyls T-stacking, as depicted by the adsorption models. (b) Upon annealing, STM images indicate intramolecular C−C bond formation between neighboring C−H and F−C sites, corresponding to the elimination of 4HF to the gas phase. Several outcomes are possible (only a few are schematically represented). (c) At higher temperature, STM indicates intermolecular bond formation. Leftover molecular C−H and F−C terminations need to be brought in close proximity via molecular diffusion for the second HF elimination step to occur (the models illustrate possible proposed outcomes). As indicated by coverage-dependent TPD, because of a higher diffusion barrier on Cu(100) than on Ag(100), the second HF loss is harder to achieve on Cu(100) for low molecular coverage. STM scale bars = 1 nm.

The C 1s and F 1s core levels measured for a monolayer of ZnTPP-m-oF8 adsorbed on Cu(100) or Ag(100) (i.e., in the blue spectra of Figure 2b) indicate that the adsorbed molecules are intact. The main C 1s feature, centered around −285 eV, possesses a triangular shape that is well reproduced by the C 1s DOS of Figure 2d calculated for molecule 1. The spectrum possesses a low binding energy component centered at −284.5 eV attributed to the pyrrolic −CH and a broad peak centered at −285.5 eV containing overlapping emission from carbons in diverse molecular environments. The presence of C−F bonds is clearly observed in the C 1s spectra as a high binding energy component found at −288 eV. For monolayers on Ag(100) and Cu(100), the intensity ratio of the main C 1s line to the C−F feature is ≈34:8 and ≈34.7:8, respectively, in good agreement with the expected molecular ratio of 36:8. The corresponding F 1s core levels of Figure 2b contain a single component at a binding energy of −688 eV, which is compatible with a unique C−F chemical environment within each monolayer, as expected for intact ZnTPP-m-oF8.

In the XPS spectra obtained at stage 2, after the first HF desorption peak has occurred (green curves in Figure 2), the spectral intensity of the F 1s core level and the C−F components of the C 1s core level are both reduced by half. Additionally, the main component of the C 1s spectra has changed shape and is more symmetric, indicating a loss of pyrrolic contribution. In the case of Cu(100), there is an additional global shift to lower binding energy, likely due to increased screening from the now planar molecules (see the STM section) able to lie closer to the Cu substrate.[36] Plots of the F 1s core level spectra extend to −680 eV to demonstrate that there is no detectable F 1s feature associated with metal fluoride (typically reported between −682 and −684 eV[37,38] as indicated by the arrows). These observations can be explained by using molecular model 2 of Figure 2c. Model 2 is the product of an intramolecular C−C bond formation between meso-phenyl ring fluorines and pyrrolic hydrogens via the elimination of 4HF (i.e., half of the original eight F atoms) in molecule 1, resulting in a spiral-like product. Note that this stereoisomer serves as an example but is not the only possible outcome of this type of reaction, as discussed below.[39]

At stage 3, after the second HF desorption peak, most C−F components have disappeared from both the C 1s and F 1s spectra of Figure 2b (red curves). At this level of comparison, the experimental spectra are well reproduced by the core level DOS of Figure 2d, which was calculated for model 3 of Figure 2c, where the four remaining fluorines have been replaced by hydrogens.

The two-step process suggested by the TPD and XPS data can be verified by using STM images of the molecular overlayers measured at reaction stages 1, 2, and 3 as shown in Figure 3. As seen in Figure 3a, ZnTPP-m-oF8 molecules self-assemble on both Cu(100) and Ag(100) surfaces in molecular islands forming typical square arrays favoring T-stacking of the meso-phenyl rings (more details of the STM study are available in the Supporting Information). On Cu(100), the ZnTPP-m-oF8 macrocycle is dark, while the meso-phenyl groups appear as bright spots. This characteristic contrast has been reported previously for NiTPPs adsorbed on Cu(100) and was attributed to the strong macrocycle−Cu(100) surface interaction leading to molecular distortion with upward pointing phenyl groups.[40] In the present case, however, F substituents induce additional intensity between the bright phenyl group features. On Ag(100), submolecular features of both the macrocycle and the meso-phenyl groups are clearly distinguishable. Note that these images were obtained for coverages smaller than one monolayer. Images obtained at stage 2, after the first HF desorption step, are shown in Figure 3b. The molecules appear planar, with little contrast between

https://doi.org/10.1021/acs.jpcc.2c00712
J. Phys. Chem. C 2022, 126, 6249−6257

the macrocycle and the meso-phenyl groups. Several molecular shapes are observed because of the formation of multiple regioisomers following intramolecular HF elimination. Some of these products are proposed at the bottom of Figure 3b. On Cu(100) the molecules appear well separated, while on Ag(100) the molecules are close to each other, and some may already have undergone intermolecular HF elimination and formed C−C bonds, consistent with the overlap of the two HF desorption peaks in Figure 2a. At stage 3, after the second HF desorption peak, nearly all molecules appear interconnected on both surfaces, shown in Figure 3c.

A better understanding of the mechanism leading to the second HF desorption feature is obtained from TPD spectra measured for increasing molecular coverage of ZnTPP-m-oF8 on these two single crystal substrates (see details of the TPD study in the Supporting Information). As shown in Figure 3c, the ratio of the area of the second desorption peak, A_2, to that of the first peak, A_1 (i.e., A_2/A_1), is constant and equal to ∼1 for Ag(100). This means that regardless of initial coverage, after the intramolecular HF loss, nearly all remaining fluorine react to form the second HF desorption peak. On Cu(100), however, A_2/A_1 is strongly dependent on molecular coverage: it is <1 for low coverage and ∼1 for near-monolayer coverage. This difference is explained by the lower molecular diffusivity on Cu(100) compared to Ag(100).[41] On Ag(100), even at low coverage, molecules of stage 2 can diffuse easily and find a partner to undergo intermolecular HF elimination. As a result, the amount of HF evolution is the same for both the intra- and intermolecular processes. On Cu(100), however, at low coverage, limited molecular diffusion prevents the alignment of favorable reaction sites for some adjacent molecules, and thus the intermolecular reaction cannot proceed. Near-complete HF elimination is only observed at high coverage on Cu(100).

Note that there are several possible ways in which neighboring molecules may align that can lead to intermolecular C−C bond formation. Some possibilities that could lead to the formation of either one or two C−C bonds (analogous to the biphenylene network studied in ref 25) are shown in Figure 3c. However, the STM resolution is not sufficiently high to discern between the two cases. Moreover, it is likely that depending on the molecular packing on the surface, not all C−F sites will be accessible, leading to some unreacted F as observed in XPS in Figure 2. Finally, as seen in Figure 2a, H_2 desorption is observed only at higher temperatures, when the surface has reached stage 3, and is the result of either intermolecular dehydrogenation or molecular decomposition.[14]

Taken together, the HF desorption spectra, XPS core level spectra, and STM molecular images provide compelling evidence for site-specific fluorine-mediated C−C bond formation. For the ZnTPP-m-oF8 molecule we propose a two-step process: (i) intramolecular HF evolution due to the close proximity of the H and F reaction sites and (ii) molecular surface diffusion which brings C−F and H−C sites of neighboring molecules in close proximity, resulting in C−C bond formation and subsequent intermolecular HF loss. The temperature difference between the two HF loss peaks is thus a good representation of the ease with which molecules diffuse on the surface of the metal. In both steps, we expect the dehydrofluorination process to be the same, requiring the presence of nearby C−F and H−C reaction sites in order for the simultaneous cleavage of C−H and F−C and subsequent release of HF.

As opposed to Cl, Br, and I, F does not seem to follow the commonly observed dehalogenation reaction path for C−C bond formation, illustrated in the top panel of Figure 4.

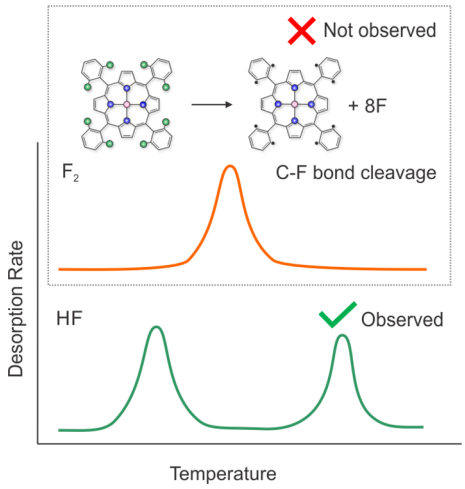

Figure 4. Dehalogenation hypothesis vs observed dehydrofluorination. A reaction mechanism involving C−F bond cleavage of all eight C−F bonds, without simultaneous C−H bond cleavage, would result in a single TPD peak, originating from a recombination of F atoms and desorption of F_2. In contrast, two HF desorption peaks are observed.

Indeed, dehalogenation would imply a one-step process leading to eight C radicals and eight F released. In such a scenario, there are two possible pathways for the released F ions: they can remain on the metal surface or be desorbed. At room temperature, excess fluorine at the surface of a metal usually leads to surface metal fluoride formation. For example, it was observed that highly fluorinated fullerenes $C_{60}F_{48}$ spontaneously deposit fluorine at the surface of Cu(100) at room temperature and readily form stable surface CuF_2.[42] Similarly, exposing a metal surface to a fluorinated species such as XeF_2 also leads to metal fluoride production through the self-terminated Mott−Cabrera mechanism, in which F^- is stabilized and attracted by its image charge in the metal surface.[43] In the work presented here, no metal fluoride is observed in XPS at any stage of the reaction. Therefore, any surface F would have to desorb immediately after the C−F bond cleavage, most likely as F_2, producing a single temperature desorption peak in TPD. Once again, we observe no evidence of a F_2 signal in TPD.

An alternative mechanism that could explain the desorption of HF instead of F_2 is the existence of a source of surface hydrogen available to react with F on the surface. Such a hydrogen source could be from a dehydrogenation reaction.[11] However, the experimental observations are not consistent with this explanation as the XPS spectra of Figure 2b contain no evidence of surface F, and the typical dehydrogenation reaction (as seen for ZnTPP) starts at temperatures higher than the observed intermolecular HF loss. Finally, an alternative path for F loss, where an H atom liberated by dehydrogenation replaces an F atom that is subsequently released to the surface, is ruled out by the design of the ZnTPP-m-oF8 molecule.[27−29]

https://doi.org/10.1021/acs.jpcc.2c00712
J. Phys. Chem. C 2022, 126, 6249−6257

A comparison to recent literature results may help in understanding possible reaction paths for dehydrofluorination. On the $TiO_2(011)$ surface, a Friedel−Crafts type mechanism was proposed for intramolecular C−C formation via HF elimination.[22] This is a sequential process where Ti sites act as a Lewis acid and promote C−F bond breaking and F abstraction by the TiO_2 surface. Then, the presence of the electron-rich π system of the nearby C−H containing ring leads to the formation of the C−C bond between the two moieties and to the release of H as a surface adsorbate. On $TiO_2(011)$, both H and F are so strongly bound to the surface that they are released only as $TiOF_x$, disrupting the $TiO_2(011)$ surface and leaving H_2O and OH residue.[20] One could imagine an analogous mechanism on a metal surface, assuming that the image charge generated by fluorine is strong enough to weaken the F−C bond. However, the mobility of F adatoms on metal surfaces is sufficiently high that it is unlikely to observe only HF as a desorption product: if H and F are not released simultaneously, the H and F atoms would likely recombine elsewhere on the surface and be released as H_2 and F_2 in addition to HF.

While identifying the elementary steps leading to simultaneous release of H and F from this molecule on these surfaces would be aided greatly by theoretical calculations, a possible route could involve the different polarizability of the C−F and C−H bonds. A more direct HF production process could involve the stabilizing effects of a C−H/F−C dipole/dipole interaction enhanced by the presence of image dipoles in the metal surface and leading to synchronous H and F release in close proximity, immediately forming volatile HF. Such a mechanism would also explain the absence of F_2 as a reaction product, as two highly polar F-bearing moieties in close proximity would be strongly repulsive. For the less polar H-terminated moieties, the repulsion would be much lower, permitting H_2 elimination and intermolecular C−C bond formation, but only at higher temperatures, as observed in Figure 2a.

Further insight into the catalytic effect of the metal surface on the dehydrofluorination process can be gained by comparing the HF and H_2 desorption spectra for ZnTPP-m-oF8 to H_2 desorption spectra for the parent molecule ZnTPP on three different metal surfaces: Cu(100), Ag(100), and Au(111), as shown in Figure 5. Au(111) has been added for direct comparison to the recent literature, reporting HF desorption upon formation of biphenylene networks on Au(111).[25] Both ZnTPP and ZnTPP-m-oF8 undergo analogous two-step reactions: an intramolecular reaction followed by an intermolecular reaction. In particular, the similarity of intramolecular reactions between either C−H/C−H or C−F/C−H bond pairs, illustrated at the top of Figure 5a, permits a direct comparison of the intramolecular HF or H_2 elimination mechanisms. H_2 desorption spectra, measured upon anneal of monolayers of ZnTPP deposited on Cu(100), Ag(100), and Au(111), are shown as the black curves in Figures 5b−d, respectively. To these are compared HF (yellow curves) and H_2 (gray curves) desorption spectra obtained upon anneal of monolayers of ZnTPP-m-oF8 on the three same metal surfaces.

For ZnTPP, the dehydrogenation mechanism is well characterized on metal surfaces and will not be discussed in detail here.[14,15] On Cu(100) and Ag(100), the spectra each possess two H_2 desorption features, the first being the product of an intramolecular reaction and the second of both

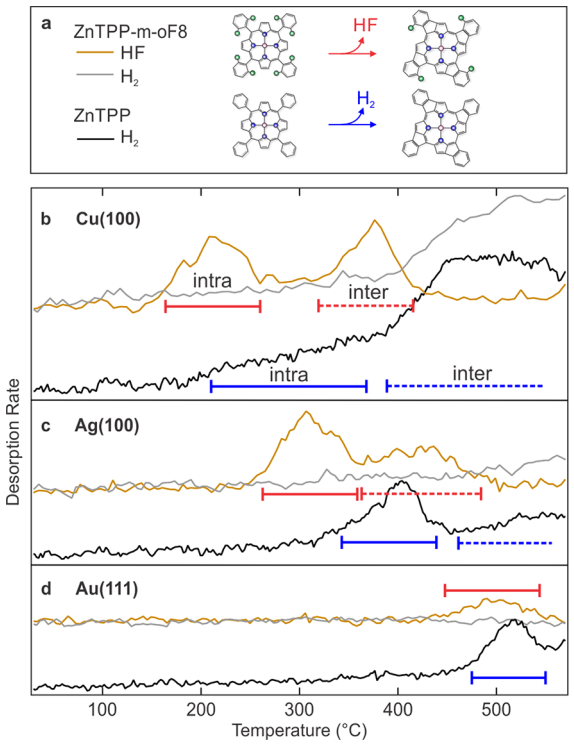

Figure 5. Metal catalytic role: ZnTPP vs ZnTPP-m-oF8. The structural similarity of the intramolecular reactions undergone by ZnTPP-m-oF8 and ZnTPP are indicated in (a). HF and H_2 desorption spectra measured for a monolayer of ZnTPP-m-oF8 are compared to H_2 desorption spectra for a monolayer of ZnTPP for the three surfaces: (b) Cu(100), (c) Ag(100), and d) Au(111), respectively. The temperature difference between the intramolecular HF elimination (red) vs intramolecular H_2 elimination (blue) is largest on Ag(100), indicating that dehydrofluorination is favored on Ag(100).

intermolecular bonding and molecular decomposition. On Au(111), only products of the intramolecular reaction are visible in the H_2 desorption spectrum as our temperature ramp did not exceed 600 °C. For ZnTPP-m-oF8, the H_2 and HF desorption features were discussed earlier for Cu(100) and Ag(100). On Au(111), only an intramolecular HF loss is measured at 500 °C, in good agreement with recently reported HF removal temperature for H and F in close proximity.[25] The HF desorption feature intensity is much smaller than that observed on Cu(100) or Ag(100) for comparable initial molecular coverage, possibly indicating an easier desorption of ZnTPP-m-oF8 molecules from Au(111) before undergoing HF elimination.

Overall, the TPD spectra indicate that the temperature necessary to achieve C−C bond formation via either dehydrofluorination or dehydrogenation for intramolecular sites is highly dependent on the metal surface. The activation energy for both reactions globally increases from Au(111), Ag(100) to Cu(100). Moreover, the temperature differences between dehydrofluorination and dehydrogenation reactions can drastically vary from one metal to another. On both Cu(100) and Au(111), Figures 5b and 5d, respectively, intramolecular reactions occur at nearly the same temperature, i.e., that both HF elimination and H_2 elimination are equally favorable on those two surfaces. This explains contradictory reports of HF elimination experiments on Au(111) in the literature. For example, Cirera et al.[24] reported no noticeable

https://doi.org/10.1021/acs.jpcc.2c00712
J. Phys. Chem. C 2022, 126, 6249−6257

preference for either H_2 removal or HF removal on Au(111). On the other hand, Fan et al.[25] observed highly selective HF elimination on Au(111), not by a chemical selectivity of HF elimination over dehydrogenation, but by utilizing a molecular precursor that self-assembles in such a way as to enforce proximity of C−H and C−F bonds and prevent proximity of C−H and C−H bonds.

Finally, HF and H_2 elimination are not always equally favorable. Our TPD experiments suggest that on Ag(100) dehydrofluorination occurs more than 100 °C lower in temperature than dehydrogenation, indicating that HF elimination is actually favored over H_2 elimination on Ag(100). This suggests that it may be possible to perform on-surface synthesis via HF elimination with much stronger chemoselectivity on Ag(100) rather than the more commonly used substrate, Au(111). In fact, previous work has even reported the opposite on Pd(111)—that H_2 elimination was indeed favored to HF elimination, allowing the use of fluorine in place of hydrogen to prevent intermolecular dehydrogenation pathways.[44]

CONCLUSION

The combined TPD, XPS, and STM studies presented here clearly show that dehydrofluorination is a viable and attractive route for targeted C−C bond formation using organic molecules on metal surfaces. Surprisingly, not only is this process possible, but it can take place at lower temperatures than analogous dehydrogenation reactions on Cu(100) and Ag(100). Moreover, this dehydrofluorination process on metal surfaces occurs as a single step, leaving no residue at the surface of the metal as HF is immediately desorbed into the gas phase. This is in contrast to approaches using a classic Ullmann coupling reaction, which requires an additional step to remove adsorbed halogens from the surface via either a high-temperature anneal or, as recently shown, a mild-temperature H exposure.[45,46] While establishing the definitive reaction mechanism requires further study, the enhanced selectivity of the dehydrofluorination reaction is achieved by involving specifically C−H/F−C pairs, rendering this C−C bond formation strategy potentially regioselective with a properly designed molecular precursor to align specific C−H/F−C pairs. For these reasons, this largely unexplored reaction could become a valuable tool for on-surface synthesis, opening new opportunities for self-assembly, unperturbed by reaction byproducts, leading to extended covalently bonded 2D organic structures with significantly enhanced long-range order.

ASSOCIATED CONTENT

Supporting Information

The Supporting Information is available free of charge at https://pubs.acs.org/doi/10.1021/acs.jpcc.2c00712.

TPD spectra as a function of molecular coverage and associated fits; XPS core level spectra and methodology for coverage calibration; STM analysis; anneal of a ZnTPP-m-oF8 multilayer (PDF)

AUTHOR INFORMATION

Corresponding Author

Sylvie Rangan − *Department of Physics and Astronomy and Laboratory for Surface Modification, Rutgers University, Piscataway, New Jersey 08854, United States;* orcid.org/0000-0002-2367-5356; Email: rangan@physics.rutgers.edu

Authors

Jonathan Viereck − *Department of Physics and Astronomy and Laboratory for Surface Modification, Rutgers University, Piscataway, New Jersey 08854, United States;* orcid.org/0000-0001-6320-6362

Yang Zhang − *Chemistry Department, Rutgers University, Newark, New Jersey 07102, United States*

Elena Galoppini − *Chemistry Department, Rutgers University, Newark, New Jersey 07102, United States;* orcid.org/0000-0003-0833-7436

Robert A. Bartynski − *Department of Physics and Astronomy and Laboratory for Surface Modification, Rutgers University, Piscataway, New Jersey 08854, United States*

Complete contact information is available at: https://pubs.acs.org/10.1021/acs.jpcc.2c00712

Author Contributions

J.V., S.R., R.A.B., and E.G. conceived the study and designed the experiment; Y.Z. performed the synthesis of the molecule; J.V. and S.R. performed XPS, STM, TPD experiments and DFT calculations; all authors were involved in writing.

Notes

The authors declare no competing financial interest.

The data that support the findings of this study are available from the corresponding author upon reasonable request.

ACKNOWLEDGMENTS

The authors acknowledge the National Science Foundation under Award No. CHE-1904648 (R.A.B. and S.R.) and CHE-1904654 (E.G.) for funding this study as well as the Laboratory for Surface Modification (LSM) and the Office of Advanced Research Computing (OARC) at Rutgers, The State University of New Jersey, for providing access to facilities that have contributed to the results reported here.

REFERENCES

(1) Fan, Q.; Gottfried, J. M.; Zhu, J. Surface-catalyzed C−C Covalent Coupling Strategies Toward the Synthesis of Low-Dimensional Carbon-Based Nanostructures. *Acc. Chem. Res.* **2015**, *48*, 2484−2494.

(2) Clair, S.; de Oteyza, D. G. Controlling a Chemical Coupling Reaction on a Surface: Tools and Strategies for On-Surface Synthesis. *Chem. Rev.* **2019**, *119*, 4717−4776.

(3) Ullmann, F.; Bielecki, J. Ueber Synthesen in der Biphenylreihe. *Berichte der deutschen chemischen Gesellschaft* **1901**, *34*, 2174−2185.

(4) Xi, M.; Bent, B. E. Iodobenzene on Cu(111): Formation and Coupling of Adsorbed Phenyl Groups. *Surf. Sci.* **1992**, *278*, 19−32.

(5) Hla, S.-W.; Bartels, L.; Meyer, G.; Rieder, K.-H. Inducing All Steps of a Chemical Reaction with the Scanning Tunneling Microscope Tip: Towards Single Molecule Engineering. *Phys. Rev. Lett.* **2000**, *85*, 2777−2780.

(6) Wang, T.; Zhu, J. Confined On-Surface Organic Synthesis: Strategies and Mechanisms. *Surf. Sci. Rep.* **2019**, *74*, 97−140.

(7) Grill, L.; Hecht, S. Covalent On-Surface Polymerization. *Nat. Chem.* **2020**, *12*, 115−130.

(8) Lafferentz, L.; Eberhardt, V.; Dri, C.; Africh, C.; Comelli, G.; Esch, F.; Hecht, S.; Grill, L. Controlling On-Surface Polymerization by Hierarchical and Substrate Directed Growth. *Nat. Chem.* **2012**, *4*, 215−220.

(9) Eichhorn, J.; Nieckarz, D.; Ochs, O.; Samanta, D.; Schmittel, M.; Szabelski, P. J.; Lackinger, M. On-Surface Ullmann Coupling: The

Influence of Kinetic Reaction Parameters on the Morphology and Quality of Covalent Networks. *ACS Nano* **2014**, *8*, 7880−7889.
(10) Fan, Q.; Wang, C.; Han, Y.; Zhu, J.; Kuttner, J.; Hilt, G.; Gottfried, J. M. Surface-Assisted Formation, Assembly, and Dynamics of Planar Organometallic Macrocycles and Zigzag Shaped Polymer Chains with C−Cu−C Bonds. *ACS Nano* **2014**, *8*, 709−718.
(11) Bronner, C.; Björk, J.; Tegeder, P. Tracking and Removing Br During the On-Surface Synthesis of a Graphene Nanoribbon. *J. Phys. Chem. C* **2015**, *119*, 486−493.
(12) Dai, J.; Zhao, W.; Xing, L.; Shang, J.; Ju, H.; Zhou, X.; Liu, J.; Chen, Q.; Wang, Y.; Zhu, J.; et al. Dechlorinated Ullmann Coupling Reaction of Aryl Chlorides on Ag(111): A Combined STM and XPS Study. *ChemPhysChem* **2019**, *20*, 2367−2375.
(13) DiSanto, G.; Sfiligoj, C.; Castellarin-Cudia, C.; Verdini, A.; Cossaro, A.; Morgante, A.; Floreano, L.; Goldoni, A. Changes of the Molecule-Substrate Interaction upon Metal Inclusion into a Porphyrin. *Chem. - Eur. J.* **2012**, *18*, 12619−12623.
(14) Rockert, M.; Franke, M.; Tariq, Q.; Ditze, S.; Stark, M.; Uffinger, P.; Wechsler, D.; Singh, U.; Xiao, J.; Marbach, H.; Steinrück, H.-P.; Lytken, O. Coverage-and Temperature-Dependent Metalation and Dehydrogenation of Tetraphenylporphyrin on Cu(111). *Chem. - Eur. J.* **2014**, *20*, 8810.
(15) Wiengarten, A.; Lloyd, J. A.; Seufert, K.; Reichert, J.; Auwärter, W.; Han, R.; Duncan, D. A.; Allegretti, F.; Fischer, S.; Oh, S. C.; et al. Surface-Assisted Cyclodehydrogenation; Break the Symmetry, Enhance the Selectivity. *Chem. - Eur. J.* **2015**, *21*, 12285−12290.
(16) Ruffieux, P.; Wang, S.; Yang, B.; Sánchez-Sánchez, C.; Liu, J.; Dienel, T.; Talirz, L.; Shinde, P.; Pignedoli, C. A.; Passerone, D.; et al. On-Surface Synthesis of Graphene Nanoribbons with Zigzag Edge Topology. *Nature* **2016**, *531*, 489−492.
(17) Zhang, Y.; Zhang, Y.; Li, G.; Lu, J.; Lin, X.; Du, S.; Berger, R.; Feng, X.; Müllen, K.; Gao, H.-J. Direct Visualization of Atomically Precise Nitrogen-Doped Graphene Nanoribbons. *Appl. Phys. Lett.* **2014**, *105*, 023101.
(18) Amsharov, K. Y.; Kabdulov, M. A.; Jansen, M. Highly Efficient Fluorine-Promoted Intramolecular Condensation of Benzo[c]-phenanthrene: A New Prospective on Direct Fullerene Synthesis. *Eur. J. Org. Chem.* **2009**, *2009*, 6328−6335.
(19) Amsharov, K. Y.; Merz, P. Intramolecular Aryl-Aryl Coupling of Fluoroarenes Through Al_2O_3-Mediated HF Elimination. *J. Org. Chem.* **2012**, *77*, 5445−5448.
(20) Kolmer, M.; Zuzak, R.; Steiner, A. K.; Zajac, L.; Engelund, M.; Godlewski, S.; Szymonski, M.; Amsharov, K. Fluorine-Programmed Nanozipping to Tailored Nanographenes on Rutile TiO_2 Surfaces. *Science* **2019**, *363*, 57−60.
(21) Kolmer, M.; Steiner, A.-K.; Izydorczyk, I.; Ko, W.; Engelund, M.; Szymonski, M.; Li, A.-P.; Amsharov, K. Rational synthesis of atomically precise graphene nanoribbons directly on metal oxide surfaces. *Science* **2020**, *369*, 571−575.
(22) Amsharov, K. Cyclodehydrofluorination of Fluoroarenes on Metal Oxides: Toward Bottom-Up Synthesis of Carbon Nanostructures on Insulating Surfaces. *Phys. Status Solidi B* **2016**, *253*, 2473−2477.
(23) Sen, D.; Błoński, P.; Torre, B. d. l.; Jelínek, P.; Otyepka, M. Thermally Induced Intra-Molecular Transformation and Metalation of Free-Base Porphyrin on Au(111) Surface Steered by Surface Confinement and Ad-Atoms. *Nanoscale Adv.* **2020**, *2*, 2986−2991.
(24) Cirera, B.; de la Torre, B.; Moreno, D.; Ondráček, M.; Zbořil, R.; Miranda, R.; Jelínek, P.; Écija, D. On-Surface Synthesis of Gold Porphyrin Derivatives via a Cascade of Chemical Interactions: Planarization, Self-Metalation, and Intermolecular Coupling. *Chem. Mater.* **2019**, *31*, 3248−3256.
(25) Fan, Q.; Yan, L.; Tripp, M. W.; Krejčí, O.; Dimosthenous, S.; Kachel, S. R.; Chen, M.; Foster, A. S.; Koert, U.; Liljeroth, P.; et al. Biphenylene Network: A Nonbenzenoid Carbon Allotrope. *Science* **2021**, *372*, 852−856.
(26) Tebi, S.; Paszkiewicz, M.; Aldahhak, H.; Allegretti, F.; Gonglach, S.; Haas, M.; Waser, M.; Deimel, P. S.; Aguilar, P. C.; Zhang, Y.-Q.; et al. On-Surface Site-Selective Cyclization of Corrole Radicals. *ACS Nano* **2017**, *11*, 3383−3391.
(27) Hayashi, H.; Yamaguchi, J.; Jippo, H.; Hayashi, R.; Aratani, N.; Ohfuchi, M.; Sato, S.; Yamada, H. Experimental and Theoretical Investigations of Surface-Assisted Graphene Nanoribbon Synthesis Featuring Carbon-Fluorine Bond Cleavage. *ACS Nano* **2017**, *11*, 6204−6210.
(28) Ohtomo, M.; Jippo, H.; Hayashi, H.; Yamaguchi, J.; Ohfuchi, M.; Yamada, H.; Sato, S. Interpolymer Self-Assembly of Bottom-up Graphene Nanoribbons Fabricated from Fluorinated Precursors. *ACS Appl. Mater. Interfaces* **2018**, *10*, 31623−31630.
(29) Panighel, M.; Quiroga, S.; Brandimarte, P.; Moreno, C.; Garcia-Lekue, A.; Vilas-Varela, M.; Rey, D.; Sauthier, G.; Ceballos, G.; Peña, D.; et al. Stabilizing Edge Fluorination in Graphene Nanoribbons. *ACS Nano* **2020**, *14*, 11120−11129.
(30) Zhang, Y.; Viereck, J.; Rangan, S.; Bartynski, R. A.; Galoppini, E. Synthesis and Study of Fluorine-Functionalized ZnTPPs. *J. Porphyrins Phthalocyanines* **2022**, DOI: 10.1142/S1088424622500146.
(31) Schmidt, M. W.; Baldridge, K. K.; Boatz, J. A.; Elbert, S. T.; Gordon, M. S.; Jensen, J. H.; Koseki, S.; Matsunaga, N.; Nguyen, K. A.; Su, S.; et al. General Atomic and Molecular Electronic Structure System. *J. Comput. Chem.* **1993**, *14*, 1347−1363.
(32) Lee, C.; Yang, W.; Parr, R. G. Development of the Colle-Salvetti Correlation-Energy Formula into a Functional of the Electron Density. *Phys. Rev. B* **1988**, *37*, 785−789.
(33) Becke, A. D. Density-Functional Thermochemistry. III. The Role of Exact Exchange. *J. Chem. Phys.* **1993**, *98*, 5648−5652.
(34) Hehre, W. J.; Ditchfield, R.; Pople, J. A. Self-Consistent Molecular Orbital Methods. XII. Further Extensions of Gaussian-Type Basis Sets for Use in Molecular Orbital Studies of Organic Molecules. *J. Chem. Phys.* **1972**, *56*, 2257−2261.
(35) Horcas, I.; Fernández, R.; Gómez-Rodríguez, J. M.; Colchero, J.; Gómez-Herrero, J.; Baro, A. M. WSXM: A Software for Scanning Probe Microscopy and a Tool for Nanotechnology. *Rev. Sci. Instrum.* **2007**, *78*, 013705.
(36) When the molecule becomes planar, the phenyl groups rotate in plane and no longer prevent the π system from getting closer to the substrate. As a result, the molecular levels are subjected to greater screening from the metallic electrons: this is observed by the slight lowering of the binding energy of the photoelectron peaks. Compared to calculations, the experimental photoemission peak just after the first intramolecular HF loss is shifted to lower binding energy with respect to its expected position.
(37) Vasquez, R. P. CuF_2 by XPS. *Surf. Sci. Spectra* **1993**, *2*, 155−159.
(38) Wolan, J. T.; Hoflund, G. B. Surface Characterization Study of AgF and AgF_2 Powders Using XPS and ISS. *Appl. Surf. Sci.* **1998**, *125*, 251−258.
(39) Ruggieri, C.; Rangan, S.; Bartynski, R. A.; Galoppini, E. Zinc(II) Tetraphenylporphyrin on Ag(100) and Ag(111): Multilayer Desorption and Dehydrogenation. *J. Phys. Chem. C* **2016**, *120*, 7575−7585.
(40) Zamborlini, G.; Luftner, D.; Feng, Z.; Kollmann, B.; Puschnig, P.; Dri, C.; Panighel, M.; Di Santo, G.; Goldoni, A.; Comelli, G.; Jugovac, M.; Feyer, V.; Schneider, C. M. Multi-Orbital Charge Transfer at Highly Oriented Organic/Metal Interfaces. *Nat. Commun.* **2017**, *8*, 1−8.
(41) Bieri, M.; Nguyen, M.-T.; Gröning, O.; Cai, J.; Treier, M.; Aït-Mansour, K.; Ruffieux, P.; Pignedoli, C. A.; Passerone, D.; Kastler, M.; et al. Two-Dimensional Polymer Formation on Surfaces: Insight into the Roles of Precursor Mobility and Reactivity. *J. Am. Chem. Soc.* **2010**, *132*, 16669−16676.
(42) Petukhov, M. N.; Oreshkin, A. I.; Muzychenko, D. A.; Oreshkin, S. I. Fluorination of Cu(001) Surface by $C_{60}F_{48}$ Molecule Adsorption. *J. Phys. Chem. C* **2020**, *124*, 347−355.
(43) Qiu, S. R.; Lai, H.-F.; Yarmoff, J. A. Self-Limiting Growth of Metal Fluoride Thin Films by Oxidation Reactions Employing Molecular Precursors. *Phys. Rev. Lett.* **2000**, *85*, 1492−1495.

(44) Wang, C.-X.; Jin, Q.; Shu, C.-H.; Hua, X.; Long, Y.-T.; Liu, P.-N. Dehydrogenative Homocoupling of Tetrafluorobenzene on Pd(111) via Para-Selective C-H Activation. *Chem. Commun.* **2017**, *53*, 6347−6350.
(45) Abyazisani, M.; MacLeod, J. M.; Lipton-Duffin, J. Cleaning Up After The Party: Removing the Byproducts of On-Surface Ullmann Coupling. *ACS Nano* **2019**, *13*, 9270−9278.
(46) Zuzak, R.; Jančařík, A.; Gourdon, A.; Szymonski, M.; Godlewski, S. On-Surface Synthesis with Atomic Hydrogen. *ACS Nano* **2020**, *14*, 13316−13323.

https://doi.org/10.1021/acs.jpcc.2c00712
J. Phys. Chem. C 2022, 126, 6249−6257